



Faceting and metal-exchange catalysis in (010) β -Ga₂O₃ thin films homoepitaxially grown by plasma-assisted molecular beam epitaxy

Cite as: APL Mater. **7**, 022511 (2019); <https://doi.org/10.1063/1.5054386>

Submitted: 31 August 2018 . Accepted: 02 November 2018 . Published Online: 14 December 2018

P. Mazzolini, P. Vogt , R. Schewski , C. Wouters , M. Albrecht , and O. Bierwagen 

COLLECTIONS

 This paper was selected as Featured



View Online



Export Citation



CrossMark

ARTICLES YOU MAY BE INTERESTED IN

MOCVD grown epitaxial β -Ga₂O₃ thin film with an electron mobility of 176 cm²/V s at room temperature

APL Materials **7**, 022506 (2019); <https://doi.org/10.1063/1.5058059>

Impact of proton irradiation on conductivity and deep level defects in β -Ga₂O₃

APL Materials **7**, 022510 (2019); <https://doi.org/10.1063/1.5054826>

Epitaxial lateral overgrowth of α -Ga₂O₃ by halide vapor phase epitaxy

APL Materials **7**, 022503 (2019); <https://doi.org/10.1063/1.5051058>




Faceting and metal-exchange catalysis in (010) β -Ga₂O₃ thin films homoepitaxially grown by plasma-assisted molecular beam epitaxy



Cite as: APL Mater. 7, 022511 (2019); doi: 10.1063/1.5054386
Submitted: 31 August 2018 • Accepted: 2 November 2018 •
Published Online: 14 December 2018



P. Mazzolini,¹ P. Vogt,¹  R. Schewski,²  C. Wouters,²  M. Albrecht,²  and O. Bierwagen¹ 

AFFILIATIONS

¹Paul-Drude-Institut für Festkörperelektronik, Leibniz Institut im Forschungsverbund Berlin e.V, Hausvogteiplatz 5-7, 10117 Berlin, Germany

²Leibniz-Institut für Kristallzüchtung, Max-Born-Str. 2, 12489 Berlin, Germany

ABSTRACT

We here present an experimental study on (010)-oriented β -Ga₂O₃ thin films homoepitaxially grown by plasma assisted molecular beam epitaxy. We study the effect of substrate treatments (i.e., O-plasma and Ga-etching) and several deposition parameters (i.e., growth temperature and metal-to-oxygen flux ratio) on the resulting Ga₂O₃ surface morphology and growth rate. *In situ* and *ex-situ* characterizations identified the formation of (110) and $\bar{1}10$ -facets on the nominally oriented (010) surface induced by the Ga-etching of the substrate and by several growth conditions, suggesting (110) to be a stable (yet unexplored) substrate orientation. Moreover, we demonstrate how metal-exchange catalysis enabled by an additional In-flux significantly increases the growth rate (>threefold increment) of monoclinic Ga₂O₃ at high growth temperatures, while maintaining a low surface roughness (rms < 0.5 nm) and preventing the incorporation of In into the deposited layer. This study gives important indications for obtaining device-quality thin films and opens up the possibility to enhance the growth rate in β -Ga₂O₃ homoepitaxy on different surfaces [e.g., (100) and (001)] via molecular beam epitaxy.

© 2018 Author(s). All article content, except where otherwise noted, is licensed under a Creative Commons Attribution (CC BY) license (<http://creativecommons.org/licenses/by/4.0/>). <https://doi.org/10.1063/1.5054386>

Their variety of functional properties makes semiconducting oxides appealing for applications in the broad field of opto- and microelectronics.¹ Among them, gallium oxide in its thermodynamically stable monoclinic crystal structure (β -Ga₂O₃) has recently been attracting attention in the scientific community. Its wide energy bandgap ($E_g \approx 4.7$ eV),² the possibility to adjust its electrical properties via extrinsic dopants from semi-insulating to conductive with electron concentrations in excess of $n = 10^{19}$ cm⁻³,³ and the availability of bulk β -Ga₂O₃ single crystals⁴⁻⁶ provide a great potential for the application of β -Ga₂O₃ in power electronics with higher performance than its mostly investigated competitors SiC and GaN.⁷ In addition, this material is nowadays proposed for several other applications, such as deep UV detectors,⁸ heterojunction solar cells,⁹ and memristive switching devices.¹⁰ Nonetheless, the development of gallium oxide is still in its early stage and the full understanding of the physical

mechanisms ruling its functional properties is crucial to unveil its full potential.

In order to fulfill this task, it is necessary to synthesize Ga₂O₃ thin films characterized by a high crystalline order, allowing at the same time the control of the material structure at the atomic scale. In this regard, the availability of high-quality single crystalline β -Ga₂O₃ substrates with different surface orientations [e.g., (100), (001), and (010)] enables the homoepitaxial growth of high-quality thin films by different techniques, such as metal-organic chemical vapor deposition and molecular beam epitaxy (MBE).⁷ In particular, the homoepitaxy of (010)-oriented β -Ga₂O₃ thin films has been shown to have definitive advantages over the other growth surfaces because of a reduced amount of planar defects [i.e., stacking faults and twins on the (100) orientation],¹¹ a larger thermal conductivity in the [100]-direction than in other directions (important for heat dissipation in devices),¹²

and a larger growth rate with respect to the (100) and (001) cleavage planes evidenced in MBE depositions.¹³ Vogt and Bierwagen¹⁴ have previously studied and successfully described the MBE growth kinetics of Ga₂O₃ (and more in general of oxides possessing volatile suboxides) as a process in which the competing desorption of the volatile Ga₂O is ruling the growth rate of the solid Ga₂O₃ as a function of the growth temperature and the metal-to-oxygen flux ratio. Moreover, the exposure of a Ga₂O₃ surface to a Ga-flux at a sufficiently high substrate temperature (while no oxygen is provided) results in the decomposition of the solid oxide into its volatile suboxide (Ga₂O) which consequently desorbs, i.e., in the etching of the layer with a well-defined rate as a function of the employed metal flux.¹⁵ The ability to selectively remove the first layers of Ga₂O₃ before the homoepitaxial deposition is appealing for the fabrication of devices;^{16,17} in fact, it can remove a Si contamination in Ga₂O₃ homoepitaxy that is commonly found at the substrate-film interface and possibly results in the formation of a parallel parasitic channel detrimental for planar devices.¹⁶

In comparison to Ga₂O₃, the MBE growth of In₂O₃ has a kinetic advantage by a higher oxidation efficiency of In and a lower desorption of the suboxide (In₂O).¹⁸ The growth of (In, Ga)₂O₃, in contrast, is characterized by a thermodynamically preferred incorporation of Ga over In into the film.¹⁹ A significant increase of the growth rate during Ga₂O₃ MBE on a β -Ga₂O₃(201) buffer layer on the Al₂O₃(0001) substrate has been observed in the presence of an additional In-flux.²⁰ As a consequence, it has been observed that the orthorhombic phase of gallium oxide (i.e., ϵ -Ga₂O₃) can be formed.²⁰ Instead of being incorporated into the film, this In-flux promoted the Ga₂O₃ growth by metal-exchange catalysis, a collaborative effect of the kinetic advantage of In₂O₃ growth and the thermodynamic advantage of Ga incorporation.²⁰ A similar behavior has been observed using an additional Sn-flux during the MBE of Ga₂O₃ on Al₂O₃(0001).²¹

In this work, we investigate the effect of (i) substrate treatments, (ii) MBE growth parameters, and (iii) an additional In-flux on the surface morphology and deposition rate of homoepitaxial (010)-oriented β -Ga₂O₃ thin films. Notably, we show the formation of (110) and ($\bar{1}\bar{1}0$)-facets on the nominally oriented (010) surface after both a Ga-etching of the bulk crystal and homoepitaxial depositions at sufficiently high growth temperatures ($T_g \geq 700$ °C). Moreover, we give the first demonstration of a significantly increased growth rate of β -Ga₂O₃(010) films grown on β -Ga₂O₃(010) substrates by an additional In-flux during the deposition process ($\Gamma = 2.8$ nm/min, i.e., more than threefold with respect to the same deposition conditions without supplying In) at high growth temperature ($T_g = 900$ °C). This metal-exchange catalyzed Ga₂O₃ is grown in the monoclinic phase, has a low surface roughness (root mean square - rms < 0.5 nm), and is not evidencing significant In-incorporation.

The samples were deposited in an MBE system equipped with an O-plasma source run at an RF-power of 300 W.

O-flows between 0.33 and 1 standard cubic centimeter per minute (sccm) were supplied to the plasma cell. Commercial β -Ga₂O₃ (010) insulating (Fe-doped) and n-type (Sn-doped) substrates purchased from Tamura Corporation were used for this study. All the substrates were In-bonded on a Si carrier wafer and the internal thermocouple temperature (placed between the heater and the carrier wafer) is considered as T_g . The metal fluxes were measured as the beam equivalent pressures (BEPs) prior the treatments/depositions using a nude ion gauge filament placed in the growth position. The metal fluxes are also expressed in terms of particle fluxes [ϕ_{Me} (nm⁻² s⁻¹)] by measuring the growth rate under O-rich deposition conditions on the Al₂O₃(0001) substrates (i.e., full metal incorporation).¹⁵ The surface treatments and the thin film growth were *in situ* monitored by reflection high-energy electron diffraction (RHEED, Createc GmbH) at an electron energy of 20 keV. The surface morphology was characterized by atomic force microscopy (AFM, Bruker Dimension Edge) in the PeakForce tapping mode. The composition of the sample deposited in the presence of an additional In-flux was investigated with scanning electron microscope-based energy dispersive X-ray (EDX) spectroscopy (Zeiss ULTRA 55). The homoepitaxial layers were monitored by X-ray diffraction (XRD) symmetric, out-of-plane $2\theta-\omega$ scans (PANalytical X'Pert Pro MRD) and by means of transmission electron microscopy (TEM—aberration corrected FEI Titan 80-300 operating at 300 kV). Scanning TEM (STEM) images were recorded with a high-angle annular dark-field (HAADF) detector with an inner acceptance angle of 35 mrad and a camera length of 196 mm. TEM samples were prepared and studied in cross section view perpendicular to the [001] direction.

- (i) **Substrate treatments.** Prior to the deposition, we investigated the role of two different treatments on the (010) surface of Fe:Ga₂O₃ substrates: O-plasma performed in a T_g window 700–900 °C at an O-flux of 1 sccm for a time of $t = 30$ min, and a Ga-etching using a Ga-flux ($BEP_{Ga} = 4.9 \times 10^{-7}$ mbar, i.e., $\Phi_{Ga} = 5.6$ nm⁻² s⁻¹) at $T_g = 800$ °C without additional oxygen for $t = 30$ min. Based on our previous observation on heteroepitaxially grown β -Ga₂O₃ (201) oriented thin films on sapphire (0001), this Ga-etching process should result in the removal of approximately ≈ 140 nm Ga₂O₃ from the substrate surface.¹⁵

Figure 1(a) shows the AFM image of a (010) Ga₂O₃ substrate surface before thermal treatment (after solvent cleaning). The surface appears featureless and shows a low surface roughness (rms = 0.19 nm). Wet chemical etching in 85 wt.% H₃PO₄ at 130 °C for 15 min, which should have removed ≈ 300 nm,²² followed by an annealing treatment in 1 bar of O₂ at 950 °C for 60 min produced a similar morphology as shown in Fig. 1(b).

An O-plasma treatment performed at high temperatures is a common procedure to clean the Ga₂O₃ substrate surface before the MBE deposition.²³ This was not found to affect the surface morphology and the rms [see Fig. 1(c)]

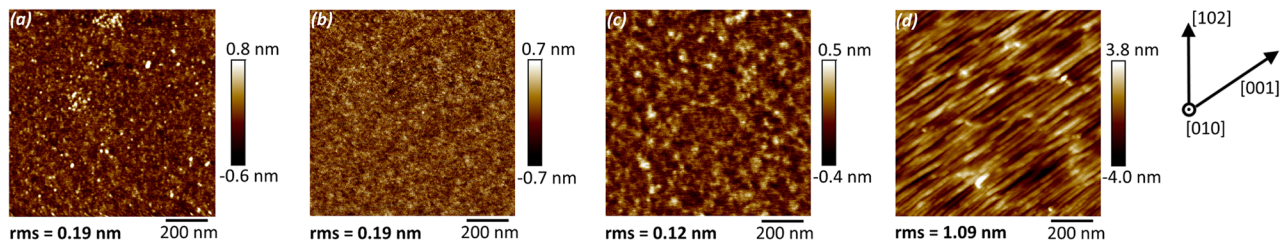


FIG. 1. Surface AFM images ($1 \times 1 \mu\text{m}^2$) of (a) solvent cleaned, (b) wet etched + 1 bar O-annealed ($T = 950 \text{ }^\circ\text{C}$), (c) O-plasma treated ($T = 800 \text{ }^\circ\text{C}$), (d) Ga-etched ($T = 800 \text{ }^\circ\text{C}$) Fe:Ga₂O₃ substrates.

independently on the T_g of the treatment (700–900 °C). The RHEED patterns recorded along the [001] and $[\bar{1}00]$ azimuthal directions of the O-plasma treated sample [Figs. 2(a) and 2(b), respectively] showed the presence of streaks which become more defined after the treatment with respect to the untreated substrate (not shown), in agreement with what has been observed by Okumura *et al.*²³ Since this treatment was found to be beneficial and at the same time was not affecting the Ga₂O₃ surface morphology, an O-plasma cleaning process at a substrate temperature of 800 °C (1 sccm O-flow, $t = 30$ min) has been performed prior to all the depositions and the Ga-etching experiment.

The (010) surface after the Ga-etching, shown in Fig. 1(d), exhibits the appearance of elongated features oriented along the [001] direction which result in an overall roughening ($\text{rms} = 1.09 \text{ nm}$). A similarly oriented morphology for (010) β -Ga₂O₃ has recently been observed by Sasaki *et al.* with substrates annealed in N₂ at 1000 °C²⁴ and by Baldini *et al.* for homoepitaxially grown thin films deposited via metal organic vapor phase epitaxy (MOVPE).²⁵ Line profiles extracted orthogonally to the [001] direction in the AFM images acquired after the Ga-etching treatment [Figs. 3(a) and 3(b), respectively] allowed us to extract the angle between the (010) surface and the lateral sides of the elongated features;

this was found to be between 9° and 15°, similar from both the sides [red dashed lines in Fig. 3(a)].

The RHEED pattern acquired *in situ* after the Ga-etching process showed an increment in the intensity of the streaks with respect to the O-plasma treatment, especially visible along the $[\bar{1}00]$ azimuth [Fig. 2(d)]; the interspacing among the streaks remained unchanged with respect to the O-plasma treatment. Nonetheless, the RHEED pattern acquired along the [001] azimuth [i.e., along the direction of the elongated features visible in Figs. 1(d) and 3(b)] shows the presence of wedges, consisting of weak oblique streaks [Fig. 2(c)]. We assign these wedges to the presence of facets oriented parallel to the RHEED azimuth and normal to the oblique streaks.²⁶ The angle between the oblique streaks and the substrate surface normal of $\approx 14^\circ$ allows us to identify these facets as (110) and $(\bar{1}10)$ [Fig. 2(e)], in agreement with the indicative range of inclination angles extracted from the AFM line profiles (Fig. 3(a)). Both surfaces are symmetry equivalent. The proposed structure in Fig. 2(e) follows the rules by Bermudez,²⁷ i.e., considering stoichiometric surfaces that contain all 5 atoms. The presence of (110) and $(\bar{1}10)$ facets after the reported Ga-etching treatment [Fig. 1(d)] or an annealing in N₂,²⁴ and their absence after our O-plasma treatment or annealing in 1 bar O₂ [Figs. 1(c) and 1(b), respectively] suggests that the (110)

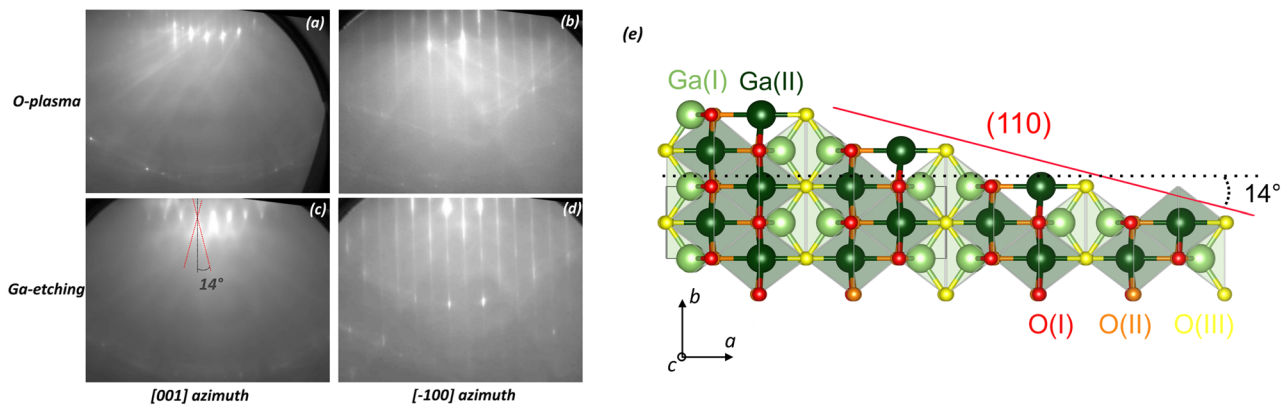


FIG. 2. RHEED patterns of O-plasma treated [(a) and (b)] and Ga-etched [(c) and (d)] β -Ga₂O₃ (010) substrates taken along [001] and $[\bar{1}00]$ azimuthal directions [(a),(c) and (b),(d), respectively]. The red dotted lines reported in (c) are a guide for the eye to highlight the presence of wedges. (e) β -Ga₂O₃ atomic model.

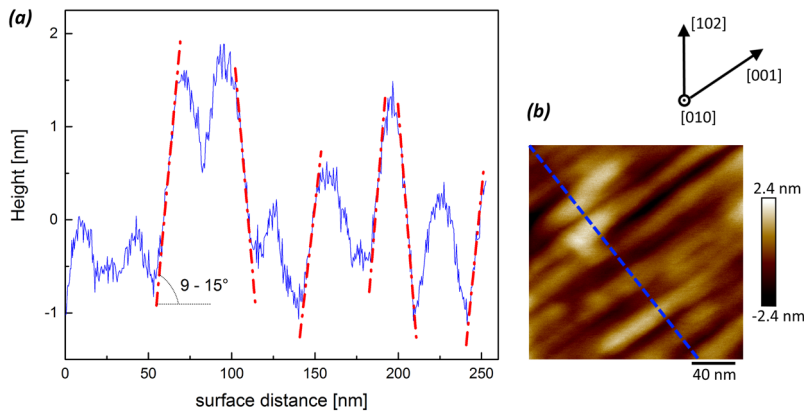


FIG. 3. Line profile (not to scale) extracted orthogonally to the [001] direction from an AFM $200 \times 200 \text{ nm}^2$ image of the Ga-etched (010) Fe:Ga₂O₃ substrate [same sample shown in Fig. 1(d)]. The blue dotted line on the AFM image is evidencing where the line profile shown in the graph has been extracted. The red dotted lines in the graph are guides for the eyes evidencing the lateral profile of the [001]-oriented features for which the angle with respect to the (010) surface has been extracted.

and $\bar{1}10$ β -Ga₂O₃ surfaces are thermodynamically more stable with respect to the (010) surface under metal-rich/oxygen-poor (i.e., reducing) conditions. A qualitatively similar observation of the preferred formation of (111) surfaces/facets under oxygen-rich, but (100) surfaces/facets under indium-rich/oxygen-poor growth conditions during MBE of In₂O₃ has been related to the strong dependence of the anisotropy of the In₂O₃ surface free energy on oxygen chemical potential²⁸ predicted by first principles calculations.²⁹ Applied to β -Ga₂O₃, this would relate the (positive) free energies E_{110} and E_{010} of the (110) and (010) surfaces, respectively, as $E_{110}/\cos(14^\circ) > E_{010}$ under O-rich conditions and $E_{110}/\cos(14^\circ) < E_{010}$ under Ga-rich conditions, with the factor $1/\cos(14^\circ)$ describing the increased surface area due to the faceting.

The identification of the (110) and $\bar{1}10$ facets induced on the (010) β -Ga₂O₃ surface by the Ga-etching is a particularly relevant observation in view of device fabrication since this treatment is proposed prior the thin film deposition in order to eliminate contaminations from the substrate interface.^{16,17}

(ii) Homoepitaxial depositions. For all the samples, the same Ga-flux ($\text{BEP}_{\text{Ga}} = 1.9 \times 10^{-7} \text{ mbar}$, i.e., $\Phi_{\text{Ga}} = 2.2 \text{ nm}^{-2} \text{ s}^{-1}$) and deposition time ($t = 30 \text{ min}$) was employed.

The incorporation of all provided Ga would result in a β -Ga₂O₃ film thickness of about 105 nm and a growth rate of 3.5 nm/min. The AFM images of a series of β -Ga₂O₃ thin films deposited at an O-flow of 0.33 sccm in the temperature window 600–900 °C are reported in Figs. 4(a)–4(d). This corresponds to a slightly metal-rich deposition condition.¹⁴

For a T_g of 600 °C, we evidenced the appearance of islands on the (010) surface [Fig. 4(a)]. The 3-dimensional growth obtained under these deposition conditions is also suggested by the appearance of spots in the RHEED patterns acquired during growth (not shown). For sufficiently high deposition temperatures [i.e., $T_g \geq 700 \text{ °C}$ —Figs. 4(b)–4(d)], we observe a smoother surface with elongated features oriented in the [001] direction, similar to the Ga-etched substrate [Fig. 1(d)] and the MOVPE-grown, homoepitaxial (010) thin films by Baldini

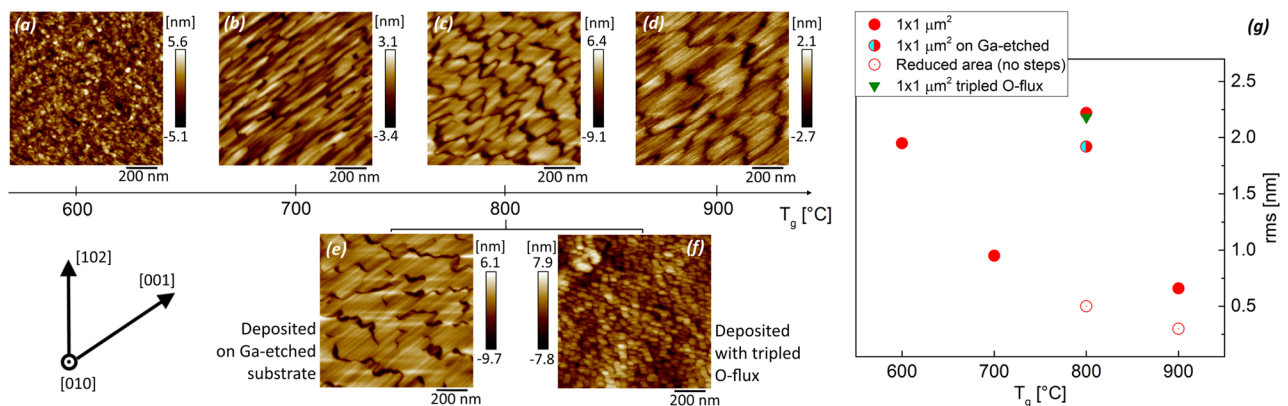


FIG. 4. AFM acquisitions of homoepitaxial Ga₂O₃ thin films deposited for $t = 30 \text{ min}$ on Fe:Ga₂O₃ (010) substrates at (a) $T_g = 600 \text{ °C}$, (b) $T_g = 700 \text{ °C}$, (c) $T_g = 800 \text{ °C}$, and (d) $T_g = 900 \text{ °C}$ with the same metal and oxygen fluxes. (e) and (f) are both deposited at $T_g = 800 \text{ °C}$, but on top of a Ga-etched substrate and with tripled O-flux, respectively (on Sn:Ga₂O₃ substrate). The extracted rms as a function of T_g is reported in (g).

*et al.*²⁵ Moreover, we also highlight for the samples deposited at 800 and 900 °C the presence of higher steps almost orthogonal to the [001] direction. The typical spacing among them is in the range of ≈ 200 nm, while the height is found to be lower for higher T_g (in the range of 10 nm and 5 nm for $T_g = 800$ °C and 900 °C, respectively). We hypothesize that the origin of these additional features could be related to the (unintentional) miscut angle of the Fe:Ga₂O₃ substrates and/or the limited diffusion length of the growing species. Without considering the aforementioned steps [i.e., throughout the selection of smaller areas in the AFM micrographs reported in Figs. 4(c) and 4(d)], the surface roughness of the films deposited under metal rich conditions is found to decrease with increasing T_g [Fig. 4(g)]. For instance, for the sample deposited at 900 °C, the rms is around 0.3 nm without considering the steps ($\approx 120 \times 120$ nm² extracted areas) and 0.66 nm for the full area of 1×1 μm^2 [Fig. 4(d)]; these two points are reported in Fig. 4(g) as an empty dotted and a filled red circle, respectively.

The RHEED acquired during the depositions performed at $T_g \geq 700$ °C evidenced the presence of the same patterns as shown in Fig. 2. As in the case of the Ga-etching process, under these conditions the intensity of the RHEED increased immediately after the opening of the metal shutter. The TEM analysis performed in the c-projection of the homoepitaxial layers deposited at $T_g \geq 700$ °C under slightly metal-rich conditions is showing the formation of the same (110) and $(\bar{1}10)$ faceted surface (see Fig. 5) previously evidenced after the Ga-etching process. Nevertheless, the RHEED pattern collected along the [001] direction was not showing clear wedges as in the case of the Ga-etched substrate [Fig. 2(c)]. We hypothesize that this could be related to the formation of less pronounced facets in the case of the homoepitaxial films with respect to the Ga-etching treatment.

Moreover, we performed a deposition at $T_g = 800$ °C on top of the previously Ga-etched substrate [showed in Fig. 1(d)] in order to investigate the effect of an already induced faceted surface on the homoepitaxial growth. The AFM scan collected after the deposition is reported in Fig. 4(e): the surface morphology and the rms are both very similar to its twin sample deposited on top of the un-etched Ga₂O₃ crystal [Figs. 4(c) and 4(g)]. Therefore, the very different substrate surface morphologies before deposition [see Figs. 1(c) and 1(d)] for the

O-plasma and the Ga-treated substrate, respectively] did not affect the morphology of the deposited film.

Furthermore, we switched the deposition conditions to the O-rich regime by tripling the O-flow (i.e., 1 sccm), while maintaining constant the Ga-flux with a $T_g = 800$ °C. This deposition has been made on a Sn:Ga₂O₃ substrate. Similarly to the sample deposited at 600 °C, the RHEED pattern acquired during growth showed the appearance of spots and the resulting surface [Fig. 4(f)] is characterized by the presence of 3-d islands with rms exceeding 2 nm [green triangle in Fig. 4(g)]. Based on these results, we conclude that the formation of facets on the (010) β -Ga₂O₃ surfaces is related to Ga-rich conditions (in both depositions and etching treatments) at sufficiently high substrate temperatures ($T_g \geq 700$ °C). This evidence opens the possibility of homoepitaxial growth of β -Ga₂O₃ thin films on (110)-oriented substrates, a crystal orientation which has not yet been studied in the literature.

The evaluation of the growth rate for homoepitaxially grown thin films is not trivial due to the very same nature of substrate and film. Nevertheless, the presence of a defective regrowth interface and/or a small change of the unit cell parameters due to a slightly different composition between the substrate and the deposited film has already been showed in the literature to result in the appearance of XRD “Pendellösung” fringes (whose spacing is inversely proportional to the layer thickness) in the vicinity of the (020) β -Ga₂O₃ reflection in $2\theta-\omega$ scans.^{23,30} For the homoepitaxially grown samples reported in this work, we could identify clear thickness fringes just for the samples deposited in Ga-rich conditions at $T_g \geq 700$ °C (Fig. 6).

From the bright field TEM images acquired for some of these samples we can confirm the overall thickness of the homoepitaxially grown thin films extracted from XRD data [e.g., sample deposited at $T_g = 900$ °C in Fig. 7(a)]. Moreover, we notice that the interface between the epitaxial layer and the substrate is visible as a dark line. The origin of this contrast is not clear up to now, but indicates strain located at the interface. This confirms the presence of a disturbed interface layer that locally breaks the symmetry of the crystal, eventually resulting in the Pendellösung fringes in the X-ray data.

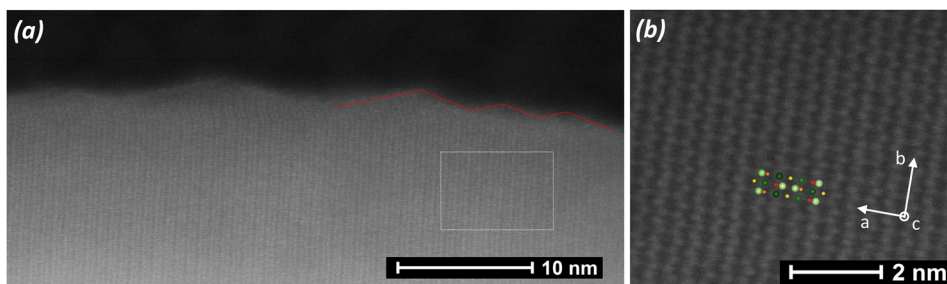


FIG. 5. HAADF-STEM images in the c-projection of the homoepitaxial Ga₂O₃ layer deposited at $T_g = 700$ °C in (a) showing the (110) and $(\bar{1}10)$ faceting on the growth surface (red lines as guidelines); (b) is a high-magnification image of the indicated region in (a) with an overlay of the same Ga₂O₃ atomic model showed in Fig. 2(e).

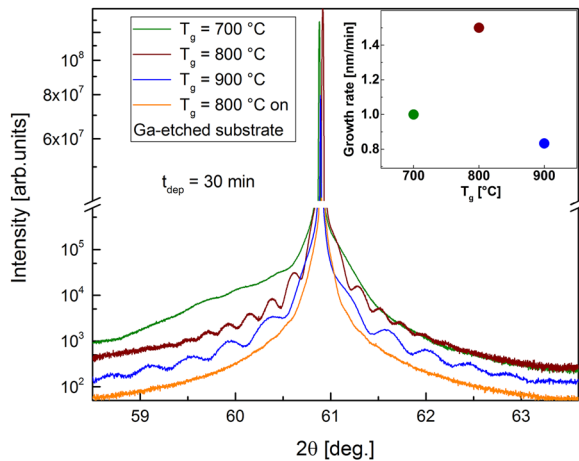


FIG. 6. XRD of the (020) reflection of homoepitaxially grown Ga_2O_3 thin films deposited with the same metal and oxygen fluxes at $T_g = 700\text{--}800\text{--}900\text{ }^\circ\text{C}$ for $t = 30$ min (green, bordeaux, and blue curves, respectively). The orange line is referring to the homoepitaxial samples grown at $T_g = 800\text{ }^\circ\text{C}$ on top of a Ga-etched substrate. In the inset graph, the growth rate extracted from the distance among their thickness fringes as a function of the deposition temperature is reported.

Nevertheless, the sample deposited at $800\text{ }^\circ\text{C}$ on top of the Ga-etched crystal (orange curve in Fig. 6) does not show the presence of well-defined fringes, in contrast to its twin sample deposited on top of the O-plasma treated substrate (bordeaux curve in Fig. 6). This could be connected to the removal of the defective interface from the Ga_2O_3 substrate surface (i.e., Ga-etching treatment) or to the induced rougher interface on which the deposition started [Fig. 1(d)]. We also assume that the total lack of thickness fringes for both, the sample deposited at the lowest temperature ($600\text{ }^\circ\text{C}$) and the one deposited at $800\text{ }^\circ\text{C}$ in O-rich conditions, could be connected to their rough surface [Figs. 4(a) and 4(f)].

Looking at the inset graph reported in Fig. 6, we notice that the growth rate of slightly Ga-rich deposition conditions is found to increase with increasing T_g from $700\text{ }^\circ\text{C}$ (1 nm/min) to $800\text{ }^\circ\text{C}$ (1.5 nm/min), while decreasing again to its lowest value for a further increase of the substrate temperature to $900\text{ }^\circ\text{C}$ (0.8 nm/min). A qualitatively similar behavior of the growth rate as a function of T_g in the MBE Ga_2O_3 (010)-homoepitaxial growth under slightly Ga-rich rich conditions has been previously reported by Okumura *et al.*²³ This experimental findings are different from what has been previously observed for the growth kinetics studies on heteroepitaxially grown (201) $\beta\text{-Ga}_2\text{O}_3$ films;^{14,15,18,19} in this case, under Ga-rich deposition conditions, the growth rate was found to decrease while increasing T_g due to the favorable desorption of the volatile Ga_2O suboxide before its further oxidation to Ga_2O_3 . Even though a full understanding of the growth kinetics is out of the scope of this paper, we can assume that the different recorded behaviors should be related to the different nature of the (010) and (201) surfaces and its consequences on reactivity and desorption behavior and/or the different metal fluxes (i.e., growth rates) used for the different studies.

As a comparison to our results, the highest recently reported growth rates for homoepitaxial (010) $\beta\text{-Ga}_2\text{O}_3$ thin films were found to be up to $\approx 3.2\text{ nm/min}$ for plasma assisted MBE (rms < 0.5 nm),³⁰ $\approx 11\text{ nm/min}$ for ozone-based MBE (rms $\approx 0.7\text{ nm}$),¹³ $\approx 5.5\text{ nm/min}$ (rms > 10 nm) for MOVPE,²⁵ and $\approx 32\text{ nm/min}$ for low pressure chemical vapor deposition (rms $\approx 4\text{ nm}$).³¹

(iii) In-catalyzed growth. The best scenario for a device-oriented Ga_2O_3 thin film would be a smooth surface obtained at a sufficiently high growth rate.

Unfortunately, it is difficult to optimize at the same time these two requirements: while the smoother surfaces are usually obtained at high T_g [as also evidenced in this

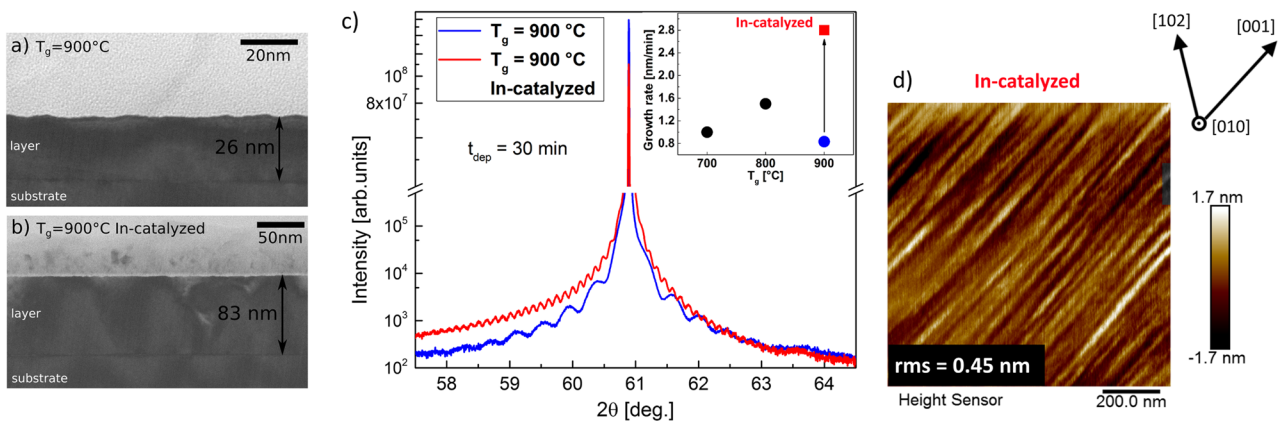


FIG. 7. TEM bright field images comparing the layer thickness of homoepitaxial Ga_2O_3 layers for (a) regular and (b) In-catalyzed growth at $T_g = 900\text{ }^\circ\text{C}$ for the same deposition time (30 min). (c) XRD of the (020) reflection of the same homoepitaxially grown layers with (red curve) and without (blue, already reported in Fig. 6) the presence of the additional In-flux during the deposition process. (d) AFM of the In-catalyzed sample (on $\text{Sn:Ga}_2\text{O}_3$ substrate).

work in Fig. 4(g)], in this conditions, the growth rate is usually limited by the desorption of the volatile Ga_2O suboxide.¹⁴ Vogt *et al.* recently identified the possibility to drastically increase the growth rate of Ga_2O_3 thin films due to metal-exchange-catalysis via the employment of an additional In-flux.²⁰ Nonetheless, this approach has only been demonstrated for heteroepitaxy associated with the formation of the orthorhombic phase of Ga_2O_3 ($\epsilon\text{-Ga}_2\text{O}_3$) on top of a $\beta\text{-Ga}_2\text{O}_3$ (201) oriented buffer layer on a sapphire (0001) substrate.²⁰ In this work we adopted the same approach, trying to evidence the effect of In-catalysis in the growth of Ga_2O_3 thin films on $\beta\text{-Ga}_2\text{O}_3$ (010).

Maintaining the same Ga and O fluxes of the slightly metal-rich deposition conditions, we grew a $\beta\text{-Ga}_2\text{O}_3$ film by metal-exchange catalysis at $T_g = 900^\circ\text{C}$ under an additional In-flux ($\text{BEP}_{\text{In}} = 1.3 \times 10^{-7}$ mbar, i.e., equal to 1/3 of the Ga flux of $2.2 \text{ nm}^{-2} \text{ s}^{-1}$). The deposition time was maintained at 30 min as in the previous depositions. Both, cross sectional TEM bright field images [Figs. 7(a) and 7(b)] and XRD $2\theta\text{-}\omega$ scans in the vicinity of the (020) peak [Fig. 7(c)] are demonstrating that the presence of In catalyzes the homoepitaxy of (010) $\beta\text{-Ga}_2\text{O}_3$ thin films, drastically increasing the growth rate to more than 3 times that of the reference film (from 0.83 nm/min to 2.8 nm/min). The growth rate in the presence of In is found to be the highest with respect to the other depositions in Me-rich conditions at $T_g \geq 700^\circ\text{C}$ [inset in Fig. 7(c)]. Indeed, almost all Ga is incorporated into the film, highlighting the potential for growth rate maximization under In-catalyzed conditions by further increasing the Ga- and O-fluxes.

Both XRD [red curve in Fig. 7(c)] and HAADF-STEM (Fig. 8) show that the metal-exchange catalysis for (010) homoepitaxy is resulting in the formation of the same monoclinic phase as the underling substrate. EDX measurements performed on the sample deposited in presence of the additional In-flux did not evidence incorporation of In into the film (i.e., <1% detection limit), in line with our previous observations on the In-catalysis of heteroepitaxial Ga_2O_3 thin films.²⁰ Moreover, we do not see the presence of an additional XRD peak at lower 2θ which would be expected in case of In-incorporation due to the formation of $(\text{In}_x\text{Ga}_{1-x})_2\text{O}_3$ alloy [red curve Fig. 7(c)].³²

A closer look by TEM at the interface between the epitaxial layer and the substrate in the bright field TEM

images [Figs. 7(a) and 7(b)] indicates the presence of faceting, especially at the interface of the layer grown without In (not shown).

Despite being the thickest, the resulting 84 nm thick In-catalyzed (010) $\beta\text{-Ga}_2\text{O}_3$ film is characterized by a low surface roughness [rms < 0.5 nm, Fig. 7(d)] solely arising from the same [001]-oriented line features as seen in the faceted Ga-etched and homoepitaxially deposited films under metal-rich conditions. The absence of the additional steps orthogonal to the [001] direction evidenced in the case of homoepitaxial films deposited on $\text{Fe:Ga}_2\text{O}_3$ substrates [see Figs. 4(c)–4(e)] is yet to be clarified. It could be related to the employment of a $\text{Sn:Ga}_2\text{O}_3$ substrate with a different (unintentional) miscut angle and/or to an increased diffusion length of the growing species promoted by the In-catalysis.³³

STEM-HAADF images acquired for the In-catalyzed sample again resolves the elongated features along the [001] direction [Fig. 7(d)] to arise from $(\bar{1}10)$ and (110) facets [Figs. 8(a) and 8(b)]. Due to the low atomic number of oxygen, exclusively Ga atoms are visible as bright dots. However, by overlaying the atomic structure of the lattice to the images we are able to distinguish between octahedrally and tetrahedrally coordinated Ga atoms. Even though these images are projections along the c -directions, we may infer the atomic surface structure from that comparison [Fig. 8(b)]. As can be seen, the structure is not in accordance with the structure shown in Fig. 2(e) [also reported as reference in Fig. 8(b)]. According to STEM, we observe exclusively tetrahedrally coordinated Ga atoms in the surface. The surface thus would not contain octahedrally coordinated Ga and four-fold coordinated oxygen atoms. However, a detailed analysis requires more experimental and theoretical work on pure (110) surfaces.

In summary, we have shown that Ga-rich conditions at sufficiently high substrate temperatures (i.e., $T_g \geq 700^\circ\text{C}$) during both Ga-etching and MBE deposition lead to ordered (010) $\beta\text{-Ga}_2\text{O}_3$ surfaces composed of $(\bar{1}10)$ and (110) shallow facets. Lower growth temperatures or vastly O-rich growth conditions result in disordered and rough surfaces. We have further demonstrated that the recently identified metal-exchange catalysis mediated by an additional In-flux during growth²⁰ strongly increases the growth rate in $\beta\text{-Ga}_2\text{O}_3$ (010) homoepitaxy at high growth temperatures while maintaining the monoclinic crystal structure, a low surface roughness

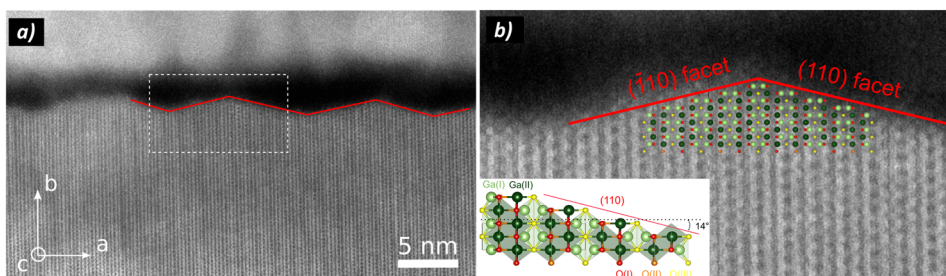


FIG. 8. HAADF-STEM images in the c -projection of the layer (a) showing the (110) and $(\bar{1}10)$ faceting on the growth surface of the sample deposited in the presence of an additional In-flux at $T_g = 900^\circ\text{C}$. (b) high-magnification image of the indicated region in (a) with an overlay of the Ga_2O_3 atomic model; in the image, it is also reported as reference the same $\beta\text{-Ga}_2\text{O}_3$ atomic model showed in Fig. 2(e).

(rms < 0.5 nm), and without significant incorporation of In. We believe that these findings can represent important steps further for the obtainment of homoepitaxial, device-quality β -Ga₂O₃ thin films by suggesting (110) to be a potentially stable substrate orientation for MBE and MOVPE growth and suggesting metal-exchange catalysis as an avenue to overcome the severe growth-rate limitations due to suboxide desorption also in MBE of (100) and (001) β -Ga₂O₃.

We would like to thank Thomas Auzelle for critically reading the manuscript, Hans-Peter Schönherr and Carsten Stemmler for technical MBE support, and Uwe Jahn for EDX measurements. This work was performed in the framework of GraFOx, a Leibniz-Science Campus partially funded by the Leibniz Association.

REFERENCES

- ¹X. Yu, T. J. Marks, and A. Facchetti, *Nat. Mater.* **15**, 383 (2016).
- ²H. H. Tippins, *Phys. Rev.* **140**, A316 (1965).
- ³M. Higashiwaki, K. Sasaki, A. Kuramata, T. Masui, and S. Yamakoshi, *Appl. Phys. Lett.* **100**, 013504 (2012).
- ⁴N. Ueda, H. Hosono, R. Waseda, and H. Kawazoe, *Appl. Phys. Lett.* **70**, 3561 (1997).
- ⁵Z. Galazka, R. Uecker, K. Irmscher, M. Albrecht, D. Klimm, M. Pietsch, M. Brützmam, R. Bertram, S. Ganschow, and R. Fornari, *Cryst. Res. Technol.* **45**, 1229 (2010).
- ⁶A. Kuramata, K. Koshi, S. Watanabe, Y. Yamaoka, T. Masui, and S. Yamakoshi, *Jpn. J. Appl. Phys., Part 2* **55**, 1202A2 (2016).
- ⁷S. J. Pearton, J. Yang, P. H. Cary, F. Ren, J. Kim, M. J. Tadjer, and M. A. Mastro, *Appl. Phys. Rev.* **5**, 011301 (2018).
- ⁸M. Orita, H. Ohta, M. Hirano, and H. Hosono, *Appl. Phys. Lett.* **77**, 4166 (2000).
- ⁹T. Minami, Y. Nishi, and T. Miyata, *Appl. Phys. Express* **6**, 044101 (2013).
- ¹⁰Y. Aoki, C. Wiemann, V. Feyrer, H.-S. Kim, C. M. Schneider, H. Ill-Yoo, and M. Martin, *Nat. Commun.* **5**, 3473 (2014).
- ¹¹R. Schewski, M. Baldini, K. Irmscher, A. Fiedler, T. Markurt, B. Neuschulz, T. Remmele, T. Schulz, G. Wagner, Z. Galazka, and M. Albrecht, *J. Appl. Phys.* **120**, 225308 (2016).
- ¹²M. Handweg, R. Mitdank, Z. Galazka, and S. F. Fischer, *Semicond. Sci. Technol.* **31**, 125006 (2016).
- ¹³K. Sasaki, A. Kuramata, T. Masui, E. G. Villora, K. Shimamura, and S. Yamakoshi, *Appl. Phys. Express* **5**, 035502 (2012).
- ¹⁴P. Vogt and O. Bierwagen, *Appl. Phys. Lett.* **108**, 072101 (2016).
- ¹⁵P. Vogt and O. Bierwagen, *Appl. Phys. Lett.* **106**, 081910 (2015).
- ¹⁶E. Ahmadi, O. S. Koksaldi, X. Zheng, T. Mates, Y. Oshima, U. K. Mishra, and J. S. Speck, *Appl. Phys. Express* **10**, 071101 (2017).
- ¹⁷Y. Oshima, E. Ahmadi, S. Kaun, F. Wu, and J. S. Speck, *Semicond. Sci. Technol.* **33**, 015013 (2018).
- ¹⁸P. Vogt and O. Bierwagen, *Appl. Phys. Lett.* **109**, 062103 (2016).
- ¹⁹P. Vogt and O. Bierwagen, *APL Mater.* **4**, 086112 (2016).
- ²⁰P. Vogt, O. Brandt, H. Riechert, J. Lähmann, and O. Bierwagen, *Phys. Rev. Lett.* **119**, 196001 (2017).
- ²¹M. Kracht, A. Karg, J. Schörmann, M. Weinhold, D. Zink, F. Michel, M. Rohnke, M. Schowalter, B. Gerken, A. Rosenauer, P. J. Klar, J. Janek, and M. Eickhoff, *Phys. Rev. Appl.* **8**, 054002 (2017).
- ²²T. Oshima, T. Okuno, N. Arai, Y. Kobayashi, and S. Fujita, *Jpn. J. Appl. Phys., Part 1* **48**, 040208 (2009).
- ²³H. Okumura, M. Kita, K. Sasaki, A. Kuramata, M. Higashiwaki, and J. S. Speck, *Appl. Phys. Express* **7**, 095501 (2014).
- ²⁴K. Sasaki, M. Higashiwaki, A. Kuramata, T. Masui, and S. Yamakoshi, *Appl. Phys. Express* **6**, 086502 (2013).
- ²⁵M. Baldini, M. Albrecht, A. Fiedler, K. Irmscher, R. Schewski, and G. Wagner, *ECS J. Solid State Sci. Technol.* **6**, Q3040 (2017).
- ²⁶A. Ichimiya and P. I. Cohen, *Reflection High-Energy Electron Diffraction* (Cambridge University Press, Cambridge, 2004).
- ²⁷V. M. Bermudez, *Chem. Phys.* **323**, 193 (2006).
- ²⁸O. Bierwagen, J. Rombach, and J. S. Speck, *J. Phys.: Condens. Matter* **28**, 224006 (2016).
- ²⁹P. Agoston and K. Albe, *Phys. Rev. B* **84**, 045311 (2011).
- ³⁰E. Ahmadi, O. S. Koksaldi, S. W. Kaun, Y. Oshima, D. B. Short, U. K. Mishra, and J. S. Speck, *Appl. Phys. Express* **10**, 041102 (2017).
- ³¹S. Rafique, M. R. Karim, J. M. Johnson, J. Hwang, and H. Zhao, *Appl. Phys. Lett.* **112**, 052104 (2018).
- ³²C. Kranert, J. Lenzner, M. Jenderka, M. Lorenz, H. von Wenckstern, R. Schmidt-Grund, and M. Grundmann, *J. Appl. Phys.* **116**, 013505 (2014).
- ³³M. Baldini, M. Albrecht, D. Gogova, R. Schewski, and G. Wagner, *Semicond. Sci. Technol.* **30**, 024013 (2015).